CrystEngComm

Accepted Manuscript

ROYAL SOCIETY OF CHEMISTRY

www.rsc.org/crystengcomm

Single-crystalline $Bi_{19}Br_3S_{27}$ nanorods with efficiently improved photocatalytic activity

Yajie Chen,[a] Guohui Tian,*[a,b] Tong Feng,[c] Wei Zhou,[a] Zhiyu Ren,[a] Taoran Han,[a] Yuting Xiao[a] and Honggang Fu,*[a]

Received (in XXX, XXX) Xth XXXXXXXXX 200X, Accepted Xth XXXXXXXXX 200X
First published on the web Xth XXXXXXXXX 200X
DOI: 10.1039/b000000x

Recently, there has been much interest in the design and development of affordable and highly efficient visible light photocatalysts that can resolve the pivotal issues concerning environmental treatment. Herein, we presented the synthesis and application of single-crystalline $Bi_{19}Br_3S_{27}$ nanorods as highly efficient photocatalyst. The $Bi_{19}Br_3S_{27}$ nanorods were prepared by a general and facile one-pot solvothermal method. The obtained $Bi_{19}Br_3S_{27}$ nanorods were characterized using X-ray diffraction, transmission electron microscopy, field emission scanning electron microscopy, and X-ray photo-electron spectroscopy. The use of cetyltrimethylammonium bromide was contributed to the formation of 1D nanorod-like superstructure. The visible light photocatalytic performance and stability of the $Bi_{19}Br_3S_{27}$ nanorods outperformed that of the corresponding Bi_2S_3 prepared without the introduction of bromine.

1. Introduction

Research In the past few years, semiconductor photocatalysis, has been widely used for the treatment of polluted water.[1,2] It is generally believed that the morphology and structure are important factors that influence the photocatalytic properties of semiconductor photocatalyst, and there are a lot of papers concerning the synthesis of the photocatalysts with different morphologies.[3-5] Among the various nanostructures, one dimensional (1D) nanostructures such as nanorods, nanowires, and nanotubes have attracted great interest for special 1D dimensionality and size which have been regarded as significant factors that may bring novel and excellent properties.[6-9] For example, metal oxides and metal sulfides.[10-12] Except for some materials with a highly anisotropic crystallographic structure, facile and large-scale synthesis of 1D nanostructures is also important for the practical application. Among these methods, solution-phase approaches, such as hydrothermal and solvothermal, have been widely applied to synthesize nanostructured materials with relatively low cost and good scalability.

Recent years, 1D wide band gap semiconductors (e.g. TiO_2, ZnO) have received considerable attention for its potential applications in solar cells, and as important photocatalysts for various oxidation and reduction reactions.[13-15] However, wide band gap photocatalysts can solely absorb the UV light, which accounts for only very small part of the overall sunlight, thus greatly limiting its practical applications. Hence, it is highly desirable to study visible light photocatalysts.[16-18] Recently, thanks to their narrow band gap and layered structure, many bismuth-containing oxide materials, such as Bi_2WO_6, Bi_2MoO_6 and $BiVO_4$ have shown admirable photocatalytic properties under visible light.[19-21] Especially because of the introduction of halogen in the compound system, bismuth oxyhalides (BiOX, X=F, Cl, Br and I) have received more attention and showed enhanced photocatalytic activity compared with the corresponding metal oxides. [22-25] Compared with bismuth-containing oxide photocatalysts, bismuth sulfide (Bi_2S_3) has drawn intensive attention for its potential applications in many areas (e.g. photocatalysis, electronic and optoelectronic devices) due to its good conductivity, thermoelectric properties and narrow band-gap (1.3 eV).[26-32] One of the biggest bottlenecks in photocatalytic application for Bi_2S_3 is its relatively low photocatalytic efficiency and easy subjection to photocorrosion during the photocatalytic reaction.[33-35] Therefore, it is of significance both in fundamental research and applied fields to overcome above problems. Inspired by the study about bismuth oxyhalides, it is of significance to explore the synthesis of bismuth sulfide halide to improve the electronic, optical, and photocatalytic properties via the introduction of halogen.[36-39] Considering the significant photocatalytic property of 1D structure semiconductors, 1D structure bismuth sulfide halide materials are expected to exhibit the superior visible light photocatalytic performance for the degradation of the organic pollutants. As far as we are aware, it is still a challenge to fabricate 1D single-crystalline $Bi_{19}Br_3S_{27}$ nanorods.

Herein, we report a general and facile one-pot solvothermal approach for the preparation of single-crystalline $Bi_{19}Br_3S_{27}$ nanorods in a binary glycerol/ethanol solvent system. The formation process of the one dimensional structure can be tuned. The introduction of bromine remarkably improves the photocatalytic efficiency and photostability of the $Bi_{19}Br_3S_{27}$ nanorods photocatalyst for the degradation of 2, 4-dichlorophenol.

2. Experimental section

2.1. Synthesis of single-crystalline $Bi_{19}Br_3S_{27}$ nanorods

In a typical experiment, 0.035 g thiourea, 0.15 g cetyltrimethylammonium bromide (CTAB), 0.008 g $Bi(NO_3)_3$•$5H_2O$ were dissolved in a mixture of 15 mL of ethanol and 5 mL of glycerol. The mixed aqueous solution was transferred to a Teflon-lined stainless-steel autoclave with a capacity of 40 mL. The sealed autoclave was heated at 130 ^oC for 6 h in an oven. After reaction, the autoclave was cooled naturally. The final black solid product was centrifuged, washed with anhydrous ethanol several times, and finally vacuum-dried at 60 ^oC for 2 h. A series of $Bi_{19}Br_3S_{27}$ samples from other different reaction times were also prepared (10 min, 0.5 h, 2 h, 10 h). To further interpretate the influence of the use of CTAB on structure change and photcatalytic activity, keeping other synthetic conditions unchanged, bare Bi_2S_3 was obtained under the same experimental conditions in the absence of CTAB.

2.2. Characterization.

The X-ray diffraction (XRD) of powder samples was examined on a Bruker D8 Advance diffractometer using Cu Ka radiation (l = 0.15405 nm, 40 kV, 100 mA). Transmission electron microscopy (TEM) and high-resolution TEM (HRTEM) images of samples were recorded in a JEOL 2100 microscope with a 200 kV accelerating voltage, scanning electron microscopy (SEM, Hitachi, S-4800). The surface elements and their electronic states of the samples were analyzed using X-ray photoelectron spectroscopy (XPS, Kratos-AXIS UL TRA DLD, Al Ka X-ray source). Nitrogen adsorption-desorption isotherms were collected on an ASAP 2420 (Micrometrics Instruments) nitrogen adsorption apparatus at 77 K. The UV-visible diffuse reflectance spectra of the samples were obtained using a UV-visible spectro-photometer (Shimadzu UV-2550).

2.3. Measurement of photocatalytic activity.

The photodegradation experiments were performed in a slurry reactor containing 100 mL of 50 mg L^{-1} 2, 4-dichlorophenol and 0.05 g of catalyst. A 150 W xenon lamp (Institute of Electric Light Source, Beijing) was used as the solar-simulated light source, and visible light was achieved by utilizing a UV cut filter ($\lambda \geq 420$ nm). Prior to light irradiation, the suspension was kept in the dark under stirring for 30 min to ensure the establishing of an adsorption/desorption equilibrium. Adequate aliquots (5 mL) of the sample were withdrawn after periodic interval of irradiation, and centrifuged at 10000 rpm for 5 min, then filtered through a Milipore filter (pore size 0.22 μm) to remove the residual catalyst particulates for analysis. The filtrates were analyzed using a UV-vis spectrophotometer (Shimadzu UV-2550).

In order to detect the active species during the photocatalytic reaction, hydroxyl ($^{\bullet}OH$) radicals produced by the photocatalysts under visible light irradiation were measured by the fluorescence method on a Fluoromax-4 Spectrophotometer (Horiba Jobin Yvon) using terephthalic acid (TA) as a probe molecule. The $^{\bullet}OH$ radical trapping experiments were carried out using the following procedure: A 5 mg portion of the sample was dispersed in 30 mL of a 5×10^{-4} M TA aqueous solution in a diluted NaOH aqueous solution (2×10^{-3} M). The resulting suspension was then exposed to visible light irradiation for 20 min. 2 mL of the suspension was collected and centrifuged to measure the maximum fluorescence emission intensity with an excitation wavelength of 315 nm. To detect the active species generated during photocatalytic reactivity, various scavengers were added into the solution of RhB, including 1.0 mM isopropanol (IPA, a quencher of •OH), 1 mM p-benzoquinone (BQ, a quencher of $O_2^{\bullet-}$) or 1 mM triethanolamine (TEOA, a quencher of h^+). A total organic carbon (TOC) analyzer (AnalytikJena, Multi N/C 2100S, Germany) was employed for mineralization degree analysis of the dye solutions. Prior to injection into the TOC analyzer, the samples were filtrated with a 0.45 ím Millipore filter. All experiments were carried out at least in duplicate. The reported values were within the experimental error range of ±3%.

3. Results and discussion

3.1. Structure and morphology analysis.

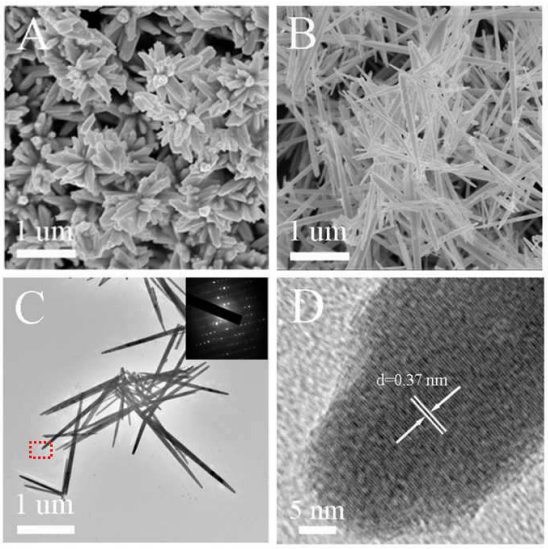

Fig. 1. (A) is the SEM image of Bi_2S_3. (B), (C), and (D) are the SEM, TEM and HRTEM images of the as-synthesized $Bi_{19}Br_3S_{27}$ nanorods, respectively; the inset in Fig. 2C shows the SAED pattern taken from the single nanorod.

The morphology and structure of the $Bi_{19}Br_3S_{27}$ are characterized by field-emission scanning electron microscopy (FESEM) and transmission electron microscopy (TEM). It can be seen that the nanorods are in large quantity (Fig 1B), which is the advantage of hydrothermal method. These nanorods are several micrometers in length and about 30 nm in diameter. The selected-area electron diffraction (SAED) pattern (inset in Fig. 1C) taken from an entire nanorod shows the single crystalline characteristics of $Bi_{19}Br_3S_{27}$ nanorods. The clear lattice image and sharp electron diffraction pattern demonstrate that nanorods retain the high crystallinity, which is reconfirmed by the HRTEM image (Fig 1D). A HRTEM image of the single nanorod (in red line frame of Fig. 1C) is

shown in Fig. 1D. The lattice spacing of 0.37 nm between adjacent lattice planes perpendicular to the growth direction of the nanorod corresponds to the *d*-spacing of (0310) planes, which indicates that the nanorod grow along the (0310) direction (*c*-axis). This result is consistent with SAED pattern in the inset in Fig, 1C. When the reaction is carried out in the absence of CTAB, only flower-like Bi_2S_3 can be obtained (Fig. 1A).

The crystallographic structure of the Bismuth Bromide Sulfide ($Bi_{19}Br_3S_{27}$) is confirmed by powder X-ray diffraction (XRD) analysis. The XRD patterns of a series of Bismuth Bromide Sulfide samples prepared from different reaction times is depicted in Fig. 2. All of the diffraction peaks can be indexed to the hexagonal $Bi_{19}Br_3S_{27}$ with lattice constants of a=15.486 and c=4.018 (JCPDS card no. 26-0813). No impurity peaks can be detected from the XRD measurement. It can be observed that the diffraction peak intensities gradually increased with the extension of the reaction time, indicating the increase of the crystallinity of the samples.

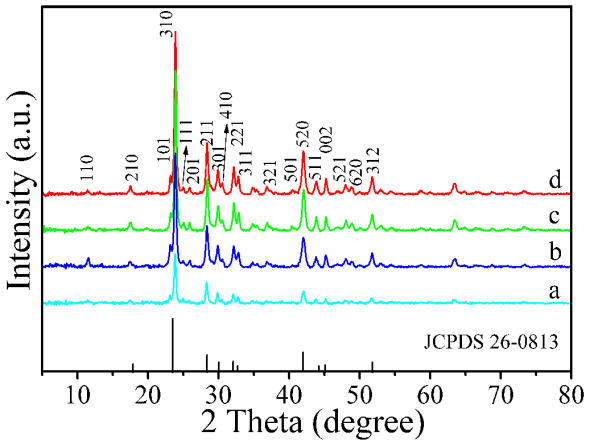

Fig. 2. XRD patterns of the prepared Bismuth Bromide Sulfide samples prepared from different reaction time: (a) 10 min, (b) 0.5 h, (c) 2 h, and (d) 6 h.

3.2. Growth process of the $Bi_{19}Br_3S_{27}$ nanorods.

In this work, the formation process of the $Bi_{19}Br_3S_{27}$ nanorods is studied. Only nanosized crystal nuclei are obtained at early stage (Fig. 3A). Then these crystal nuclei serve as subunits to grow into short 1D nanorods (Fig. 3B), and the length of nanorods gradually increase with the extension of the reaction time (Fig. 3C). Finally, long $Bi_{19}Br_3S_{27}$ nanorods with good crystallinity are formed (Fig. 3D). From the above results, it can be concluded that the formation process of the $Bi_{19}Br_3S_{27}$ nanorods mainly went through a fast nucleation and anisotropic growth process. The formation process of the $Bi_{19}Br_3S_{27}$ nanorods can be illustrated in Fig. 3E. First, $Bi(NO_3)_3$•$5H_2O$ and glycerol (Gly) form BiGly complex during the initial reaction stage. And thiourea can hydrolyze to produce active S^{2-}anions. Then the BiGly complex reacts with active S^{2-}anions to form Bi_2S_3 nanocrystals. Similarly, BiGly complex reacts with Br^- to form $BiBr_3$. Then the formed Bi_2S_3 nanocrystals react with $BiBr_3$ and nucleation started and the $Bi_{19}Br_3S_{27}$ crystalnucleus was obtained. In this study, the $Bi_{19}Br_3S_{27}$ crystallization process consists of two major events, nucleation and crystal growth. The growth rate difference of different crystal planes causes the anisotropy crystal growth. In the present work, the excess CTAB acts as capping agents and selectively adsorb onto certain crystal planes to accelerate the preferential growth. These polar crystals tend to preferentially grow along their polar direction (*c*-axes) of $Bi_{19}Br_3S_{27}$ crystal nucleus, resulting in the formation of 1D structure. With the extension of the reaction time (6 h), $Bi_{19}Br_3S_{27}$ nanorods can be obtained. In order to explain the role of glycerol, we did the control experiment without the use of glycerol in the reaction system. From the corresponding XRD pattern (Fig. S1), we can see that $Bi_{19}Br_3S_{27}$ nanorods can also be prepared, but the nanorods are not uniformed (Fig. S2B), and the length and diameter of nanorods have greatly difference with nanorods prepared with the use of glycerol (Fig. S2A). The BET surface areas (Fig. S3) of $Bi_{19}Br_3S_{27}$ samples prepared from 10 min, 0.5 h, 2 h, and 6 h were 25.3 $m^2\ g^{-1}$, 21.1 $m^2\ g^{-1}$, 18.1 $m^2\ g^{-1}$, and 16.1 $m^2\ g^{-1}$, respectively. Obviously, the gradual increase of the crystal size causes the decrease of the surface area. The control sample Bi_2S_3 has a surface area of 14.5 $m^2\ g^{-1}$.

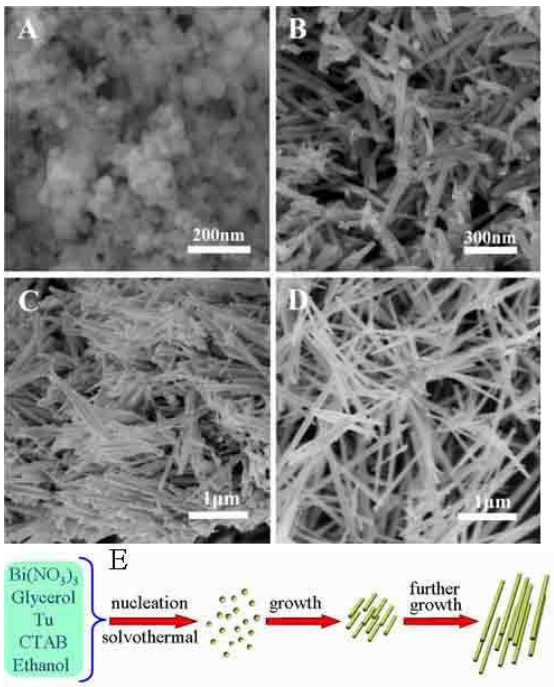

Fig. 3. (A), (B), (C), (D) are the SEM images of the obtained $Bi_{19}Br_3S_{27}$ samples prepared from 10 min, 0.5 h, 2 h, and 6 h, respectively; (E) is the schematic illustration of the growth process of the $Bi_{19}Br_3S_{27}$ nanorods.

3.3. UV-vis diffuse reflectance spectrum and XPS analysis.

The corresponding UV-vis reflectance spectrum of the $Bi_{19}Br_3S_{27}$ nanorods is shown in Fig. 4. There shows a strong photoabsorption in the visible-light region. The band gap of the synthesized $Bi_{19}Br_3S_{27}$ can be estimated from the plot in the inset of Fig. 4. The intercept of the tangent to the x-axis will give a good approximation of the band gap energy for the $Bi_{19}Br_3S_{27}$ nanorods. The estimated band gap energy of the $Bi_{19}Br_3S_{27}$ nanorods was calculated to be about 1.49 eV. Therefore, it can easily be activated by visible-light for photocatalytic decomposition of organic contaminants.

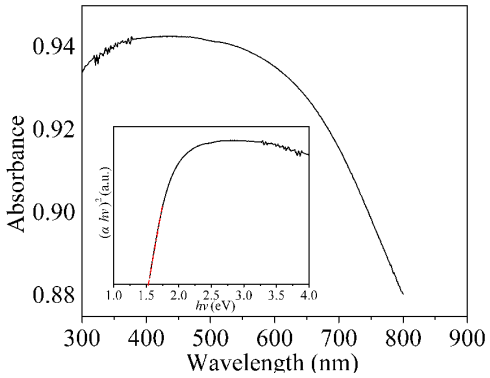

Fig. 4. UV-vis diffuse reflectance spectrum of the as-synthesized $Bi_{19}Br_3S_{27}$ nanorods and the inset is the plot of the $(\alpha hv)^{1/2}$ vs photon energy (hv).

X-ray photoelectron spectroscopy (XPS) was used to investigate the surface valence state and the chemical composition of $Bi_{19}Br_3S_{27}$. The wide spectrum (Fig. 5A) of $Bi_{19}Br_3S_{27}$ reveals the predominant presence of sulfur, bismuth, and bromine. High-resolution scans of the S element in Fig. 5B reveal several weak peaks centered at around 160.5 eV, which can be accordingly assigned to binding energies of $S2p_{3/2}$. High-resolution scan of the S element in Fig. 5C is attributed to the S2s. The results prove the existence of the S^{2+} species. Moreover, the high-resolution XPS spectra (Fig. 5B, D) show that the binding energies of $Bi4f_{7/2}$, $Bi4f_{5/2}$, $Br3d_{3/2}$ and $Br3d_{5/2}$ peaks at 158.0 eV, 163.2 eV, 67 eV and 69 eV, respectively.[37,38] The atomic ratio of Br:Bi:S here is 1:6.5:8.9, which is in line with the molar ratio of Br:Bi:S (1:6.3:9) in the as-synthesized sample. The valence band top of $Bi_{19}Br_3S_{27}$ was also measured by valence band XPS (Fig. S4). The edge of the maximum energy is at 1.20 eV below the Fermi energy. Since the optical band gap of $Bi_{19}Br_3S_{27}$ is 1.49 eV (Fig. 4 inset), the conduction band (CB) minimum would occur at -0.29 eV. The electrons on the CB edge are good reductants that can capture O_2 to generate $\bullet O_2^-$ because the CB edge potential of $Bi_{19}Br_3S_{27}$ is more negative than $EO_2/\bullet O_2^-$ (−0.28 V vs SHE).[39] These $\bullet O_2^-$ radicals are important oxidizing species responsible for the degradation of 2,4-Dichlorophenol.

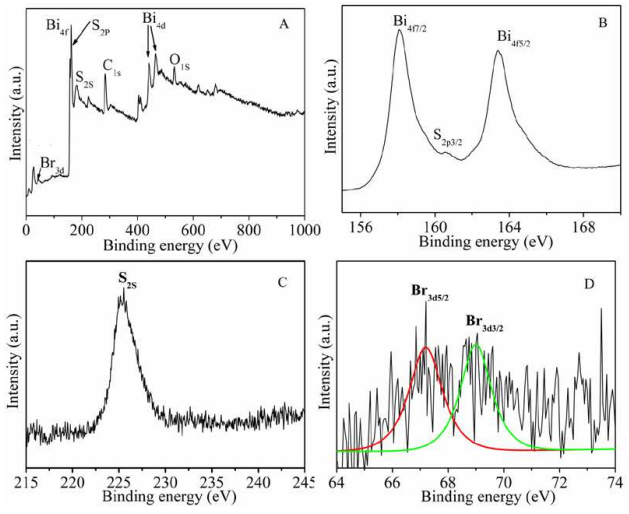

Fig. 5. Survey XPS spectrum (A), and high-resolution XPS spectra of Bi_{4f} and S_{2p} (B), S_{2s} (C) and Br_{3d} (D) of the prepared $Bi_{19}Br_3S_{27}$ nanorods.

3.4. Photocatalytic activity.

As we know, the morphology and component of photocatalysts have great influence on their photocatalytic properties. Herein, we try to get clear information about the influence of the introduction of Br on the photocatalytic properties of $Bi_{19}Br_3S_{27}$ nanorods. The control samples, the Bi_2S_3 prepared without the introduction of CTAB was also used as photocatalysts. The photocatalytic activities of the prepared photocatalysts were evaluated for the degradation of 2,4-Dichlorophenol under visible-light irradiation. As can be seen from Fig. 6A, after visible light irradiation for 3 h, the degradation fractions of 2,4-Dichlorophenol for the Bi_2S_3 nanoflowers is 28.8%. In contrast, the degradation fractions for $Bi_{19}Br_3S_{27}$ samples prepared from 10 min, 0.5 h, 2 h, 6 h and 10 h are 51.3%, 61.5%, 72.6%, 86.0%, and 85.6%, respectively. All the $Bi_{19}Br_3S_{27}$ samples exhibit significantly higher photocatalytic activity than the Bi_2S_3 nanoflowers. The above results reveal that the introduction of Bromide in the $Bi_{19}Br_3S_{27}$ remarkably improves the photocatalytic efficiency because of the interaction between charge carrier and the modified ion. Meanwhile, 1D nanostructure benefit to the quick transfer and transportation of pgotogenerated charges, so contributing to the improvement of photoctalytic activity. Moreover, the $Bi_{19}Br_3S_{27}$ samples prepared from 10 min to 6 h reaction time exhibited gradually improved photocatalytic activity due to the gradual increase of crystallinity, which can be estimated from the increase of XRD diffraction peak intensity. The increase of crystallinity can reduce the surface defects of the $Bi_{19}Br_3S_{27}$ nanorods and so decrease the recombination centers of the photogenerated electrons and holes. When the reaction time further extends, the photocatalytic activity of the obtained $Bi_{19}Br_3S_{27}$ nanorods showed no further enhancement because of the perfection of hexagonal crystal structure. The potential photocatalytic chemical process in the degradation of 2, 4-Dichlorophenol may involve several steps: When $Bi_{19}Br_3S_{27}$ nanorods were irradiated by visible light with energy greater than the band gap, electron-hole pairs would be generated and separated partially. Then some of the electrons recombined with holes while others transferred onto the surface of $Bi_{19}Br_3S_{27}$ quickly and were then captured by the adsorbed oxygen molecule to yield $\bullet O^{2-}$ and H_2O_2. Meanwhile, the •OH radical which was recognized as the reactive species responsible for the organic degradation could also be generated when $\bullet O_2^-$ interacted with H_2O_2.

The formation of •OH on the surface of photocatalysts was detected by the fluorescence technique using terephthalic acid (TA) as a probe molecule. It is well known that $^{\bullet}$OH reacts with terephthalic acid (TA) in basic solution to generate 2-hydroxy-terephthalic acid (TAOH), which emits a unique fluorescence signal with the peak centered at 426 nm. The fluorescence intensity of TAOH is proportional to the amount of •OH produced on the surface of photocatalysts. So we have detected the hydroxyl radicals indirectly by monitoring the fluorescence intensity changes of $Bi_{19}Br_3S_{27}$/TA solution. Fig. 6B shows the fluorescence spectra of $Bi_{19}Br_3S_{27}$/TA solution under visible-light irradiation, and the fluorescence intensity increases steadily with the irradiation time within 20 min. It can be concluded that

hydroxyl radicals are indeed generated on $Bi_{19}Br_3S_{27}$ under visible-light irradiation, and the rate of hydroxyl radical generation is in accordance with that of 2,4-Dichlorophenol degradation, suggesting •OH may be the main reactive species.

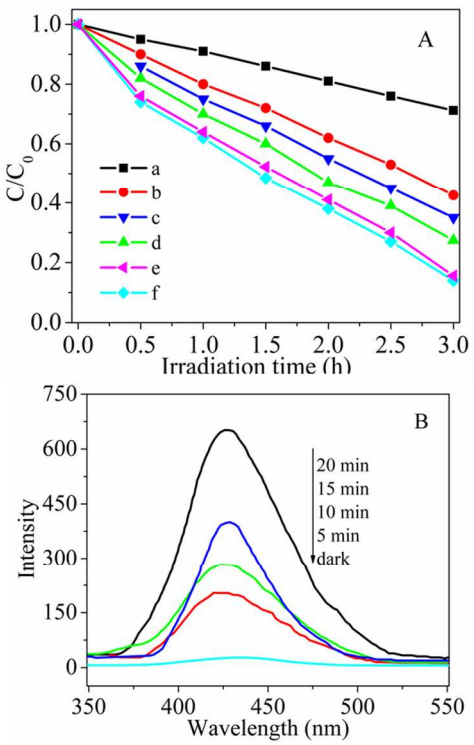

Fig. 6. (A) Visible light photocatalytic degradation curves of the 2, 4-Dichlorophenol under Bi_2S_3 (a) and $Bi_{19}Br_3S_{27}$ samples prepared from different reaction time: (b) 10 min, (c) 0.5 h, (d) 2 h, (e) 10 h, and (f) 6 h. (B) Fluorescence spectra of TAOH (2-hydroxyterephthalic acid) formed by the reaction of terephthalic acid (5×10^{-4} M, excitation at 315 nm) with •OH radicals generated from $Bi_{19}Br_3S_{27}$ nanorods (prepared from 6 h reaction time) against different irradiation time.

In order to prove the existence and role of the $•O_2^-$ reactive species, the trapping experiments of active species during the photocatalytic reaction of the $Bi_{19}Br_3S_{27}$ were done. As shown in Fig. S5, the photocatalytic degradation rate of 2, 4-dichlorophenol decreased obviously when benzoquinone (BQ, a scavenger of $O_2•^-$), 2-propanol (IPA, a scavenger of•OH), triethanolamine (TEOA, a scavenger of h^+) were added, respectively. Especially in the presence of 2-propanol and benzoquinone. Therefore, it can be concluded that photogenerated •OH and $O_2•^-$ are the main active species of $Bi_{19}Br_3S_{27}$ for 2, 4-dichlorophenol degradation under visible light irradiation.

In photocatalytic process, lots of studies showed that some degradation intermediates may be more toxic than the initial materials. Hence, the complete mineralization of organic components prior to wastewater discharging is very important. To investigate the mineralization degree of 2, 4-Dichlorophenol, the total organic carbon (TOC) removal during the degradation of 2, 4-Dichlorophenol by $Bi_{19}Br_3S_{27}$ nanorods under visible-light irradiation was tested. From Fig. 7A, it can be seen that the TOC removal efficiency of $Bi_{19}Br_3S_{27}$ nanorods is 76.2% for 2, 4-Dichlorophenol after 3 h visible light irradiation, which is much higher than that of the Bi_2S_3 nanoflowers. This result showed that, for the $Bi_{19}Br_3S_{27}$ nanorods, a larger degree of light-generated hole/electron pair excitation produced, leading to the generation of more • OH radicals, and in turn, greater pollutant mineralization. It further proved the obtained $Bi_{19}Br_3S_{27}$ nanorods showed strongly structure-induced enhancement of photocatalytic performance for the photodegradation of 2, 4-Dichlorophenol. Meanwhile, we also compared $Bi_{19}Br_3S_{27}$ with the Bi_2MoO_6 prepared according to our previous study.[41] The result showed the prepared $Bi_{19}Br_3S_{27}$ showed higher photocatalytic activity than Bi_2MoO_6 (Fig. S6).

The stability of photocatalyst is important for its application. To test the stability and reusability of the $Bi_{19}Br_3S_{27}$ nanorods for the photocatalytic reaction, the catalyst was reused for photocatalytic reaction 5 times under the same conditions, and the result is shown in Fig. 7B. The photocatalytic efficiency of the $Bi_{19}Br_3S_{27}$ nanorods decreases only 3% after 5 cycles. These results indicate that the $Bi_{19}Br_3S_{27}$ nanorods prepared by this facile method are stable for the photocatalytic degradation of organic pollutants, which is important for its application.

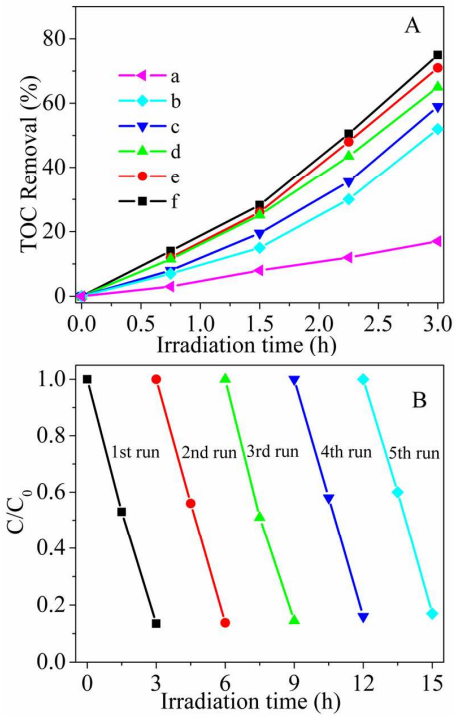

Fig. 7. (A) The profiles of total organic carbon (TOC) removals for the photodegradation of 2,4-Dichlorophenol (10 mg/L) in different aqueous catalysts, Bi_2S_3 (a) and $Bi_{19}Br_3S_{27}$ samples prepared from different reaction time: (b) 10 min, (c) 0.5 h, (d) 2 h, (e) 10 h, and (f) 6 h. (B) Repeated photocatalytic test of 2, 4-Dichlorophenol over recycled $Bi_{19}Br_3S_{27}$ nanorods under visible light irradiation.

4. Conclusions

In summary, we developed a facile one-pot solvothermal method to synthesize $Bi_{19}Br_3S_{27}$ nanorods with uniform morphology. In the synthetic process, the use of CTAB was found to play important roles, including formation of the single-crystalline hexagonal $Bi_{19}Br_3S_{27}$ nanorods,

enhancement of visible light absorption and photostability. The resulting $Bi_{19}Br_3S_{27}$ nanorods showed significantly enhanced photocatalytic activity for the degradation of 2, 4-Dichlorophenol. The new synthetic approach presented herein provides a way to control the final crystal morphology of the target $Bi_{19}Br_3S_{27}$ product. We expect to utilize this synthetic strategy to prepare other bismuth sulfide halide visible light-absorbing semiconductors.

Acknowledgments

This research was supported by the National Natural Science Foundation of China (51272070, 21371053, 21376065), Natural Science Foundation of Heilongjiang Province of China (E201455), Postdoctoral science-research developmental foundation of Heilongjiang province (LBH-Q13136).

Notes

[a] *Key Laboratory of Functional Inorganic Material Chemistry, Ministry of Education of the People's Republic of China, Heilongjiang University, Harbin 150080 P. R. China*

[b] *Key Laboratory of Chemical Engineering Process & Technology for High-efficiency Conversion, College of Heilongjiang Province, School of Chemistry and Materials Science, Heilongjiang University, Harbin 150080, China.*

[c] University of Illinois at Urbana-Champaign Department of Chemical and Biomolecular Engineer, 600 S. Mathews Ave. Urbana, Il. 61801.

Corresponding author E-mail: tiangh@hlju.edu.cn; fuhg@vip.sina.com, Tel.: +86 451 8660 4330, Fax: +86 451 8667 3647

† Electronic Supplementary Information (ESI) available: [details of any supplementary information available should be included here. See DOI: 10.1039/b000000x/

References

1 P. S. Kumar, J. Sundaramurthy, S. Sundarrajan, V J. Babu, G. Singh, S. Allakhverdiev and S. Ramakrishna, *Energy Environ. Sci.*, 2014, **7**, 3192.

2 Y. J. Wang, Q. S. Wang, X. Y. Zhan, F. M. Wang, M. Safdar and J. He, *Nanoscale,* 2013, **5**, 8326.

3 Y. Hu, X. H. Gao, L. Yu, Y. R. Wang, J. Q. Ning, S. J. Xu and X. W. Lou, *Angew. Chem. Int. Ed.* 2013, **52**, 5636.

4 Z. D. Wu, L. L. Chen, C. S. Xing, D. L. Jiang, J. M. Xie and M. Chen, *Dalton Trans.*, 2013, **42**, 12980.

5 F. J. Chen, Y. L. Cao and D. Z. Jia, *CrystEngComm*, 2013, **15**, 4747.

6 X. D. Wang, J. Xie and C. M. Li, *J. Mater. Chem. A*, 2015, **3**, 1235.

7 L. Cademartiri, G. Guerin, K. J. M. Bishop, M. A. Winnik and G. A. Ozin, *J. Am. Chem. Soc.*, 2012, **134**, 9327.

8 M. B. Sigman, Jr and B. A. Korgel, *Chem. Mater.*, 2005, **17**, 1655.

9 L. L. Long, A. Y. Zhang, Y. X. Huang, X. Zhang and H. Q. Yu , *J. Mater. Chem. A*, 2015, **3**, 4301.

10 X. T. Wang, R. Lv and K. Wang, *J. Mater. Chem. A*, 2014, **2**, 8304.

11 Z. Fang, Y. F. Liu, Y. T. Fan, Y. H. Ni, X. W. Wei, K. B. Tang, J. M. Shen and Y. Chen, *J. Phys. Chem. C*, 2011, **115**, 13968.

12 J. L. T. Chen, V. Nalla, G. Kannaiyan, V. Mamidala, W. Ji and J. J. Vittal. *New J. Chem.*, 2014, **38**, 985.

13 J. B. Mu, C.L. Shao, Z. C. Guo, Z. Y. Zhang, M. Y. Zhang, P. Zhang, B. Chen and Y. C. Liu, *ACS Appl. Mater. Interfaces*, 2011, **3**, 590.

14 H. N. Chen, Z. H. Wei, K. Y. Yan, Y. Bai and S. H. Yang, *J. Phys. Chem. Lett.*, 2014, **5**, 2890.

15 H. Tong , S. X. Ouyang , Y. P. Bi , N. Umezawa , M. Oshikiri and J. H. Ye, *Adv. Mater*., 2012, **24**, 229.

16 Y. Z. Wang, W. Wang, H. Y. Mao, Y. H. Lu, J. G. Lu, J. Y. Huang, Z. Z. Ye and B. Lu, *ACS Appl. Mater. Interfaces*, 2014, **6**, 12698.

17 Q. J. Xiang, J. G. Yu and M. Jaroniec,*Chem. Soc. Rev.*, 2012, **41**, 782.

18 L. Chen, J. He, Q. Yuan, Y. Liu, C. T. Au and S. F. Yin, *J. Mater. Chem. A*, 2015, **3**, 1096.

19 X. Li, J. G. Yu, J. X. Low, Y. P. Fang, J. Xiao and X. B. Chen, *J. Mater. Chem. A*, 2015, **3**, 2485.

20 L. Polavarapu, S. Mourdikoudis, P. Santos and J. P.-Juste, *CrystEngComm*, 2015, DOI: 10.1039/C5CE00112A.

21 J. Huang, G. Q. Tan, H. J. Ren, W. Yang, C. Xu, C. C. Zhao and A. Xia, *ACS Appl. Mater. Interfaces*, 2014, **6**, 21041.

22 H. F. Cheng, B. B. Huang, X. Y. Qin, X. Y. Zhang and Y. Dai, *Chem. Commun*., 2012, **48**, 97.

23 H. P. Jiao, X. Yu, Z. Q. Liu, P. Y. Kuang and Y. M. Zhang, *RSC Adv.*, 2015, **5**, 16239.

24 L. Q. Ye, Y. R. Su, X. L. Jin, H. Q. Xie and C. Zhang, *Environ. Sci.: Nano*, 2014, **1**, 90.

25 J. Di, J. X. Xia, S. Yin, H. Xu, L. Xu, Y. G. Xu, M. Q. He and H. M. Li, *J. Mater. Chem. A,* 2014, **2**, 5340.

26 F. Guo, Y. H. Ni, Y. Ma, N. N. Xiang and C. Liu, *New J. Chem.*, 2014, **38**, 5324.

27 Y. H. Yan, Z. X. Zhou, W. Q. Li, Y. J. Zhu, Y. Cheng, F. Y. Zhao and J. G. Zhou, *RSC Adv.*, 2014**, 4**, 38558.

28 P. Hazra, A. Jana, M. Hazra and J. Datta, *RSC Adv.*, 2014, **4**, 33662.

29 P. Lv, W. Y. Fu, H. B. Yang, H. R. Sun, Y. L. Chen, J. W. Ma, X. M. Zhou, L. C. Tian, W. J. Zhang, M. J. Li, H. Z. Yao and D. Wu, *CrystEngComm*, 2013, **15**, 7548.

30 A. A. Tahir, M. A. Ehsan, M. Mazhar, K. G. U. Wijayantha, M. Zeller and A. D. Hunter, *Chem. Mater.*, 2010, **22**, 5084.

31 Z. Q. Liu, W. Y. Huang, Y. M. Zhang and Y. X. Tong, *CrystEngComm*, 2012, **14**, 8261.

32 X. S. Rong, F. X. Qiu, J. Yan, H. Zhao, X. L. Zhu and D. Y. Yang, *RSC Adv*., 2015**, 5**, 24944.

33 L. Chen, J. He, Q. Yuan, Y. W. Zhang, F. Wang, C. T. Au and S. F. Yin , *RSC Adv.*, 2015, **5**, 33747.

34 M. Ibáñez, P. Guardia, A. Shavel, D. Cadavid, J. Arbiol, J. R. Morante and A. Cabot, *J. Phys. Chem. C*, 2011, **115**, 7947.

35 Z. W Quan, J. Yang, P. P. Yang, Z. L. Wang, C. X. Li and J. Lin, *Cryst. Growth & Design*, 2008, **8**, 200.

36 L. Y. Zhu, Y. Xie, X. W Zheng, X. Yin and X. B. Tian，*Inorg. Chem.* 2002, **41**, 4560.

37 Z. S. Aliev, S. S. M. Farhad, Y. Jafarli, I. R. Amiraslanov, A. V. Shevelkov and M. B. Babanly. *J.Alloys and Compd*., 2014, **610**, 522.

38 A. Audzijonis, R. Sereika, R. Zaltauskas and A. R. eza, *J. Phys. Chem. Solids*, 2011, **72**, 1501.

39 C. H. Deng, H. M. Guan and X. B. Tian*, Mater. Lett.*, 2013, **108**, 17.

40 Y. M.He, J. Cai, T. T. Li., Y. Wu, Y. M. Yi, M. F. Luo, L. H. Zhao, *Ind. Eng. Chem. Res.* 2012, **51**, 14729.

41 7. G. H. Tian, Y. J. Chen, W. Zhou, K. Pan, Y. Z.Dong, C. G. Tian, H. G. Fu, , *J. Mater. Chem.,* 2011, **21**, 887.

Graphical Abstract

Single-crystalline $Bi_{19}Br_3S_{27}$ nanorods were prepared and showed excellent visible light photocatalytic performance